Physica Scripta

PAPER

Mechanical, magneto-electronic and thermoelectric properties of Ba_2MgReO_6 and Ba_2YMoO_6 based cubic double perovskites: an ab initio study

RECEIVED
22 September 2023

REVISED
8 November 2023

ACCEPTED FOR PUBLICATION
27 November 2023

PUBLISHED
7 December 2023

Mohammed Elamin Ketfi[1,*], **Saber Saad Essaoud**[2,3], **Said M Al Azar**[4], **Anas Y Al-Reyahi**[5], **Ahmad A Mousa**[6,7] and **Nabil Al-Aqtash**[5]

[1] Department of Electronics, Faculty of Technology, University of M'sila, 28000 M'sila, Algeria
[2] Department of Physics, Faculty of Science, University of M'sila, 28000 M'sila, Algeria
[3] Laboratoire de Physique des Particules et Physique Statistique, Ecole Normale Supérieure-Kouba, BP 92, Vieux-Kouba, 16050 Algiers, Algeria
[4] Department of Physics, Faculty of Science, Zarqa University, 13132 Zarqa, Jordan
[5] Department of Physics, Faculty of Science, The Hashemite University, P. O. Box 330127, Zarqa, 13133, Jordan
[6] Department of Basic Sciences, Middle East University, Amman, 11831, Jordan
[7] Applied Science Research Center, Applied Science Private University, Amman, Jordan
[*] Author to whom any correspondence should be addressed.

E-mail: mohammedelamin.ketfi@univ-msila-dz

Keywords: double perovskite oxide, TB-mBJ, Seebeck Coefficient, electrical and thermal conductivity coefficients, thermal expansion coefficient

Abstract

We report an analysis of the structural, electronic, mechanical, and thermoelectric properties of oxide double perovskite structures, specifically the compounds Ba_2MgReO_6 and Ba_2YMoO_6. Our study employs first-principles density functional theory (DFT) as the investigative methodology. The electronic attributes of the examined compounds are explained by investigating their energy bands, as well as the total and partial density of states. The computational evaluation of the electronic band structure reveals that both compounds exhibit an indirect band gap semiconductor behavior in the spin-down channel, while demonstrating metallic properties in the spin-up channel. The magnetic attributes indicate a ferromagnetic nature, thus categorizing some double perovskite compounds as materials displaying half-metallic ferromagnetism (HM-FM) in addition to some other properties such as metallic and semiconductor in paramagnetic or antiferromagnetic states. The outcomes derived from the analysis of elastic constants confirm the mechanical robustness of the studied double perovskite compounds. Notably, the computed data for bulk modulus (B), shear modulus (G), and Young's modulus (E) for Ba_2MgReO_6 surpass those of Ba_2YMoO_6. The calculated ratio of Bulk to shear modulus (B/G) indicates that both compounds possess ductile characteristics, rendering them suitable for device fabrication. Furthermore, both compounds display outstanding electronic and elastic properties, positioning them as promising contenders for integration within mechanical and spintronic devices. Finally, we investigate into the thermoelectric potential by evaluating parameters such as the Seebeck coefficient, electrical conductivity, thermal conductivity, figure of merit, and power factor. This assessment is conducted using the semiclassical Boltzmann theory and the constant relaxation time approximation, implemented through the BoltzTraP code. The results indicate that the investigated double perovskite oxides hold promise for utilization in thermoelectric applications.

1. Introduction

The rising global energy demand, fueled by population growth and industrial progress, necessitates a balanced energy supply. Conventional energy sources fall short due to limitations and environmental concerns, driving exploration of alternative renewable sources. Solar energy stands out, but finding effective, cost-efficient, and

environmentally friendly materials for solar cells remains a challenge. Double Perovskite compounds have gained attention for their diverse applications including Magnetoresistance Materials [1], Catalysis [2], Solid Oxide Fuel Cells [3], Optoelectronic and thermoelectric Devices [4], High-Temperature Materials [1, 5]. Yet, their wide-bandgap oxide structure hampers optoelectronic uses [6–8]. Organic–inorganic hybrids combining organic compounds with lead halide perovskites have emerged to enhance photo-electrochemical cell efficiency. However, lead halide perovskites face issues of efficiency loss, durability, and toxicity. Halide vacancies also make them unstable. Thus, the focus is on eco-friendly, stable materials that work efficiently over time. Substituting Pb with Sn/Ge was attempted, but oxidation limited device lifetimes [9–11].

Previous studies on perovskite compounds with their various structural formations led to their being unique in having many distinctive properties, especially electronic, optical, as well as thermodynamic stability, which qualified them over others for expanded use in filters, optical devices, precise sensing devices, capacitors, and other electronic equipment.

To tackle practical challenges linked to perovskite compounds, researchers have explored double perovskite compounds with a formula $A_2B'B''X_6$. These compounds stem from the conventional perovskite structure ABX_3, known for a wide range of behaviors from insulation to superconductivity [12–18]. The perovskite structure's adaptability allows seamless integration of various elements into its lattice. Double perovskite compounds combine two simple perovskite structures (ABX_3 and $AB'X_3$) into $A_2BB'X_6$ [19–26].

Traditionally, in the context of the $A_2BB'O_6$ double perovskite compound, the A site is commonly filled by alkaline earth metals like Ca, Sr, Ba, or lanthanides like La. The B and B' positions are then occupied by transition metal elements such as Mn, Sc, Co, Ni, and others [20].

This group of materials has the potential to display various crystallographic arrangements to accommodate distinct alkaline and transition metal ions. At room temperature, these structures can take on different forms [27]: such as cubic (Fm-3m #225), seen in cases like Ba_2FeMoO_6; tetragonal (I4/m), illustrated by Sr_2CoWO_6; and monoclinic (P21/n #14), as observed in Ca_2FeMoO_6 [28].

Notably, there exist prior outstanding publications covering specific aspects of this subject. Mitchell's book [29] serves as a comprehensive resource, consolidating information about diverse perovskite and perovskite-related structures, encompassing $A_2BB'O_6$ compounds. In 1993, Anderson *et al* [30] extensively reviewed literature, cataloging 300+ instances of B-site substituted double-perovskite oxides with one or two A-site cations. Their focus was on crystal structures and, notably, the ordering of B-site cations. Cation arrangement in perovskites has been explored by King and Woodward [31], Davies *et al* [32], and Howard *et al* [33]. Goodenough [34] has covered the transport characteristics of perovskite compounds in a general sense, encompassing double perovskites. Notably, the intriguing halfmetallic and magnetoresistance traits of Sr_2FeMoO_6 and related compounds have sparked significant attention. Detailed examination of their physical attributes has been undertaken by Serrate *et al* [35], while Karppinen and Yamauchi [36] have primarily delved into their chemical aspects.

A noteworthy aspect of oxide perovskites lies in their exceptional environmental stability, rendering them more favorable for photovoltaic uses compared to other compounds. Consequently, recent research endeavors have turned toward identifying double oxide perovskites with strong light-absorbing capabilities in the visible spectrum of electromagnetic radiation. Recent work involves synthesizing $A_2BB'O_6$ (A = Ca, Sr and Ba; B, B′ = Transition Metal Elements) compounds, Investigate of Possible Half-Metallic Antiferromagnets on Double Perovskites applications It was found that A_2MoOsO_6, A_2TcReO_6, A_2CrRuO_6, where A = Ca, Sr, Ba, are all potential candidates for HM-AFM [37]. The GGA + mBJ electronic band-structure illustrates that the Ba_2FeNiO_6 is a half-metal with 100% spin polarization at the Fermi level. While Ba_2CoNiO_6 shows a ferromagnetic semiconducting nature[38]. For instance, Kubel *et al* [39] have investigated the structure of M_2NaIO_6 compounds (M = Ca, Sr, Ba). Wu [40] have presented electronic and optical characteristics of A_2FeReO_6 compounds (A = Sr, Ba), and and Sr_2MMoO_6 (M = Cr,Mn,Fe,Co) for understanding of their intriguing electronic and magnetic properties. Jeon *et al* [41] have examined the electronic structure of double perovskites, $Ba_{(2)}FeReO_{(6)}$ (metallic) and $Ca_{(2)}FeReO_{(6)}$ (insulating) using optical and x-ray absorption spectroscopy. As an alternative to lead halide perovskites, inorganic Bi-based double perovskite oxides have been suggested for diverse optoelectronic applications [42].

Many studies discussed the magnetic order of both Ba_2YMoO_6 [43–46] and Ba_2MgReO_6 [47–50] double perovskites. Recently, Hirai revealed that the Ba_2MgReO_6 has a complex magnetic structure that involves a competition between ferromagnetic and antiferromagnetic interactions [49]. The small magnetic moment of Re^{6+} does not allow for determining the magnetic order easily experimentally. Neutron spectroscopy study reveals that Ba_2YMoO_6 has a spin-liquid singlet ground state due to strong quantum effects and geometric frustration. The ground state arises from particle pairing at 2 K [46]. According to theoretical research by Chen *et al* [51], the s = 1/2 Mo^{5+} moments coexist with disordered ground states in s = 1/2 fcc systems with spin–orbit coupling.

Table 1. The atomic positions were calculated using PBE approximations of Ba_2MgReO_6 and Ba_2YMoO_6 compounds.

		GGA		
Materials	**Atoms**	**x**	**y**	**z**
$Ba_2MgReO_{6\ (Fm\text{-}3/m\ \#\ 225)}$	Ba	0,2500	0,2500	0,2500
		0.7500	0.7500	0.7500
	Mg	0,0000	0,0000	0,0000
	Re	0,5000	0, 0000	0, 0000
	O	0,7372	0,0000	0,0000
		0.2627	0.0000	0.0000
		0.0000	0,7372	0.0000
		0.0000	0.2627	0.0000
		0.0000	0.0000	0,7372
		0.0000	0.0000	0.2627
$Ba_2YMoO_{6\ (Fm\text{-}3/m\ \#\ 225)}$	Ba	0.7500	0,2500	0,2500
		0.2500	0.7500	0.7500
	Y	0,0000	0,0000	0,0000
	Mo	0,5000	0,0000	0,0000
	O	0,5000	0,0000	0,2334
		0,5000	0,0000	0,7665
		0,2334	0,5000	0,0000
		0,7665	0,5000	0,0000
		0,5000	0,2334	0,0000
		0,5000	0,7665	0,0000

The aim of this study is to assess the structural and magnetic stability of the two compounds under investigation, along with their mechanical stability. This assessment is essential to ascertain their suitability for various applications as mentioned earlier. Furthermore, we aim to explore their thermoelectric properties, particularly in light of the half-metallicity behavior observed in their electronic properties analysis.

2. Computational details

This paper employs the Full-Potential Linearized Augmented Plane Wave (FP-LAPW) method, implemented in the WIEN2k code [52], to investigate the structural, optoelectronic, and elastic properties of Ba_2MgReO_6 and Ba_2YMoO_6 based on density functional theory (DFT). For structural properties, the revised Perdew–Burke–Ernzerhof (PBE) parameterization of the generalized gradient approximation (GGA) [53] is used as the exchange–correlation functional, while the modified Becke–Johnson exchange potential [54] is utilized for optoelectronic properties. The method involves partitioning the unit cell into non-overlapping spherical muffin tins and interstitial space. To achieve energy eigenvalue convergence, the wave function in the interstitial regions is expanded using a plane wave with a cut-off of $R_{MT} \times K_{MAX} = 8$, where R_{MT} represents the minimal muffin-tin radius, and K_{MAX} is the magnitude of the maximal K vector wave in the Brillouin zone. A spherical harmonic expansion has used inside the spheres with an angular momentum up to $l_{max} = 10$. The muffin-tin radii (RMT) for Ba, Mg, Y, Re, Mo and O atoms are 1.8, 1,6, 1,7, 2,0, 1,6 and 1,5 atomic units (a.u), respectively. The valence electron configurations and core-valence separation for Ba ($6s^2$), Mg ($3s^2$), Y ($4d^1\ 5s^2$), Re ($4f^{14}\ 5d^5\ 6s^2$), Mo ($4d^5\ 5s^1$) and O ($2s^2\ 2p^4$) are provided for Brillouin zone integration. A −7.0 eV cutoff used to distinguish between valence and core states. All calculations are carried out without adding spin–orbit coupling interaction. Both total energy (10^{-5} Ry) and charge (10^{-3} e) were used as criteria for convergence during the calculation. For the estimation of the thermoelectric properties we have used the semi-local Boltzmann transport theory, implemented in the BoltzTraP code [55].

3. Results and discussion

3.1. Stability magnetic-mechanic of Ba_2MgReO_6 and Ba_2YMoO_6 compounds

To investigate Ba_2MgReO_6 and Ba_2YMoO_6 compounds, we utilized the crystallographic data from cubic double perovskites as presented by Martínez-Lope *et al* [56]. Through a comprehensive geometry optimization using the PBE functional, we obtained lattice parameters and atomic positions for Ba_2MgReO_6 and Ba_2YMoO_6 compounds. The optimized lattice parameters for both compounds are 8.0763 Å and 8.3483 Å, respectively. These double perovskite compounds adopt a cubic crystal structure with a specific space group Fm-3m (# 225)

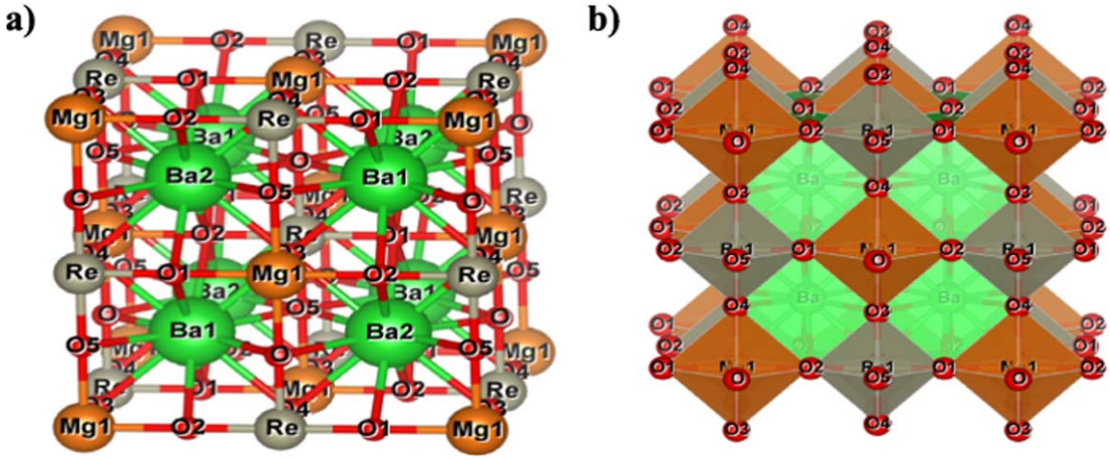

Figure 1. (a): Crystal Cubic structure of Ba_2MgReO_6 and Ba_2YMoO_6 compounds. (b): Polyhedral view along an axis.

Table 2. The calculated equilibrium lattice constants, bulk modulus, and cohesive energy for Ba_2MgReO_6 and Ba_2YMoO_6 compounds obtained by using GGA-PBE approximations.

		a (Å)	B(GPa)
	GGA	8,0763	171,0522
	Exp	8.0849 [57]	
Ba_2MgReO_6		8.179 (GGA) [48]	158.27 [48]
	GGA	8,3483	156,5235
Ba_2YMoO_6	Exp	8.3910 [57]	

as shown in figure 1. Within this structure, Ba, Mg/Y, Re/Mo, and O atoms occupy 8c (0.25, 0.25, 0.25), 4a (0, 0, 0), 4b (0.5, 0, 0), and 24e (x, 0, x) sites, respectively. Notably, the variable x takes positions at 0.2627 and 0.7372 in Ba_2MgReO_6 and 0,2334 and 0,7665 for Ba_2YMoO_6, respectively. Figure 1 illustrates the crystal structure of the both compounds. It's worth mentioning that the calculated lattice parameter for Ba_2YMoO_6 exceeds that of Ba_2MgReO_6, which could be attributed to atomic size effects.

Table 2 presents a summary of the findings and draws a comparison with alternative available data. The table illustrates that the GGA approximation produces acceptable results for both Ba_2MgReO_6 and Ba_2YMoO_2 compounds. Also, our optimized lattice parameter of Ba_2MgReO_6 is closer to experimental values than the value in reference no. [48]. The bulk modulus B(GPa), which signifies a material's ability to withstand deformation caused by hydrostatic pressure, is used to characterize these outcomes. Consequently, the Ba_2MgReO_6 compound exhibits greater resilience to external pressure due to the robust quantity and strength of atomic bonds it possesses.

Exploring how pressure influences the magnetic stability of a double perovskite oxide with varied magnetic properties such as ferromagnetic, antiferromagnetic, and paramagnetic configurations. Pressure can modify the unit cell's size, changing the lattice constant and thereby affecting the compound's magnetic stability. figure 2 shows the total energy for both Ba_2MgReO_6 and Ba_2YMoO_6 compounds versus the volume of the unit cell in different magnetic phases. The equilibrium structures exhibit ferromagnetic behavior both compounds.

Figure 3 illustrates how the total and partial magnetic moments of atoms change with variations in volume. Notably, both Ba_2MgReO_6 and Ba_2YMoO_6 maintain a consistent magnetic moment, as shown by the horizontal line, even when the volume changes. Moreover, the magnetic moments of Barium, Magnesium, and Oxygen atoms remain relatively steady while the volume gradually increases. In contrast, the magnetic moments of Rhenium, Molybdenum, and the interstitial zone exhibit some stability while experiencing a volume increase. The total magnetic moment at equilibrium volume for Ba_2MgReO_6 is consistent with that in the previous study [48]. For Ba_2YMoO_6 the previous experimental study found the magnetic moment range between $1.3 - 1.4\ \mu_B$ these values differed slightly from our results [51].

The elastic coefficients computed to evaluate the structural integrity of the compounds. Within the cubic arrangement, there exist three distinct components of the elastic tensor, namely C_{11}, C_{12}, and C_{44}. According to the obtained findings both compounds verified the criteria of mechanical stability outlined in reference [58].

$$C_{11} > 0,\ C_{44} > 0,\ C_{11} - C_{12} > 0,\ C_{11} + 2C_{12} > 0 \quad (1)$$

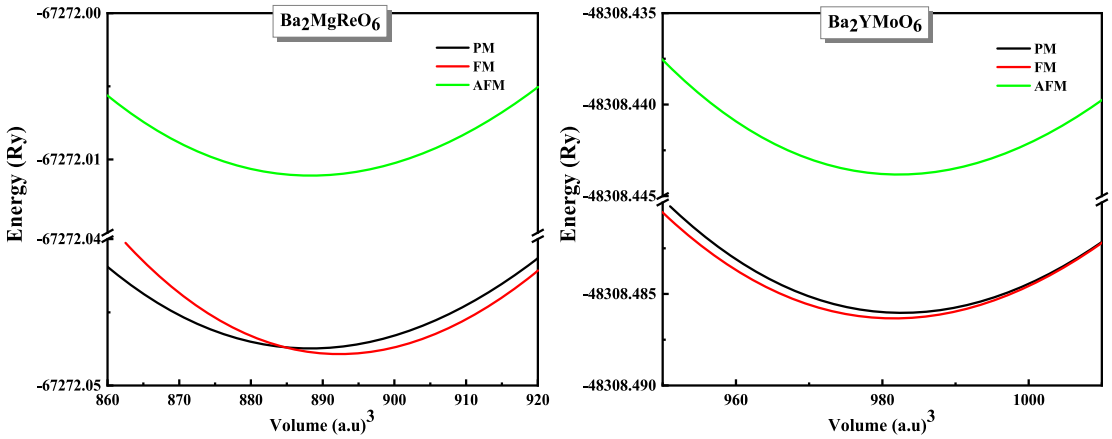

Figure 2. The total energy for compounds of Ba_2MgReO_6 and Ba_2YMoO_6 in paramagnetic, ferromagnetic and antiferromagnetic states is volume dependent.

Table 3. Elastic constants (C_{ij}), bulk modulus (B), shear modulus (G_V), Reuss shear (G_R), Pugh's ratio (B/G), Young's moduli (E), Cauchy's pressure (C'), Kleinman parameter (ξ), Poisson's ratio (υ), elastic anisotropy (A), Frantsevich's ratio (G/B), and Lame's coefficients (μ and λ) were computed for Ba_2MgReO_6 and Ba_2YMoO_6 compounds using the GGA approximation at atmospheric pressure (P = 0 GPa).

		Ba_2MgReO_6	Ba_2YMoO_6
Elastic constants	C_{11}(GPa)	232.7462	240.6328
		288.6 [48]	
	C_{12}(GPa)	135.0135	118.2988
		94.7 [48]	
	C_{44}(GPa)	82.0751	64.7970
		87.0 [48]	
Bulk modulus	B_V(GPa)	167.591	159.076
	B_R(GPa)	167.590	159.077
	B_H(GPa)	167.590	159.076
Shear modulus	G_V(GPa)	68.791	63.344
	G_R(GPa)	64.532	
		90.7 [48]	63.294
	G_H(GPa)	66.661	63.319
Young modulus	Y_V(GPa)	181.534	167.764
	Y_R(GPa)	171.573	167.647
	Y_H(GPa)	176.571	167.705
		229 [48]	
Poisson's coefficient	P_V	0.319	0.324
	P_R	0.329	0.324
	P_H	0.324	0.324
Lamés coefficients	λ	380.193	359.9715
	μ	68.8158	63.35595
Kleinman parameter	ξ	0.6912	0.61791
Anisotropy ratio	A (s.u)	1.67958	1.05934
		0.89 [48]	
Cauchy's pressure	C' (GPa)	52.9384	53.5018
Pugh's ratio	B/G	2.43621	2.5112
		1.756 [48]	

This suggests the mechanical stability of our compounds. Hence, the C_{ij} constants were derived while calculating the total energy with varying volume-conserving strains, causing the disruption of cubic symmetry. Subsequently, a range of parameters were determined, including bulk and shear modulus, Young's modulus (Y), Cauchy's pressure C″, Lame's coefficients (λ and μ), Poisson's ratio (υ), Kleinman parameter (ξ), and anisotropy constant (A).

The outcomes obtained through the Voigt Reuss Hill approximations (VRH) [59–61] have been consolidated in table 3. It's important to highlight that currently, there exist no existing experimental or prior

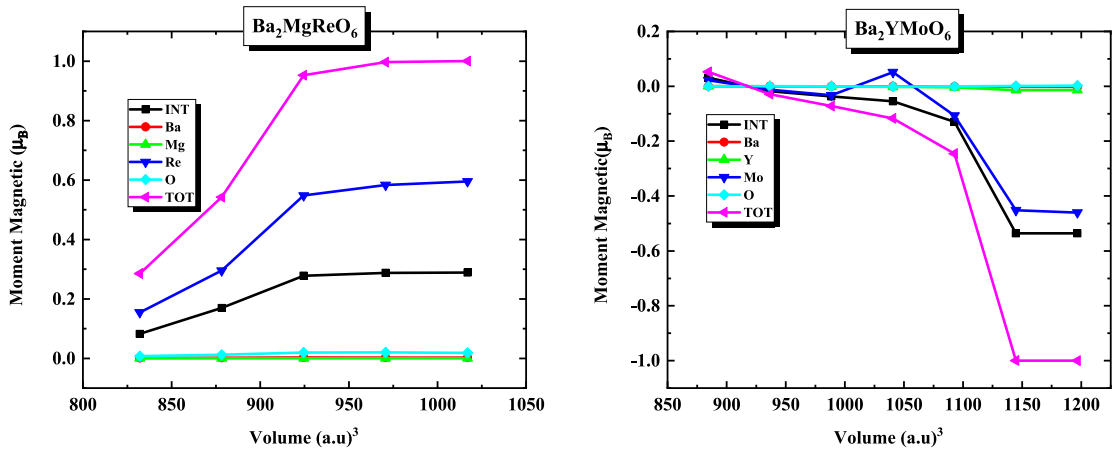

Figure 3. Total and partial magnetic moment variations as function of volume for Ba_2MgReO_6 and Ba_2YMoO_6.

theoretical findings to serve as a basis for comparison with our attained results. The mathematical connections linking the elastic constants to each of these elastic parameters are presented as follows [62]:

$$B_V = B_R = \frac{1}{3}(C_{11} + 2C_{12}) \tag{2}$$

$$G_V = \frac{1}{5}(C_{11} - C_{12} + 3C_{44}) \tag{3}$$

$$Y = \frac{9BG_V}{3B + G_V} \tag{4}$$

$$A = \frac{2C_{44}}{C_{11} - C_{12}} \tag{5}$$

$$C'' = (C_{12} - C_{44}) \tag{6}$$

$$\nu = \frac{3B - E}{6B} \tag{7}$$

$$\xi = \frac{C_{11} + 8C_{12}}{7C_{11} + 2C_{12}} \tag{8}$$

$$\lambda = \frac{Y_\nu}{(1 + \nu)(1 - 2\nu)} \tag{9}$$

$$\mu = \frac{Y}{2(1 + \nu)} \tag{10}$$

The compound Ba_2MgReO_6 exhibits a higher compressibility coefficient compared to the other one, implying a greater resistance to external pressure. Notably, for both Ba_2MgReO_6 and Ba_2YMoO_6 compounds, the bulk moduli computed from elastic constants are in strong agreement with those derived from the EOS equations (table 2).

The characterization of material rigidity can be accomplished through shear modulus (G) values, contrasting the approach used for bulk modulus. Our findings indicate that the shear modulus of Ba_2MgReO_6 is greater than that of Ba_2YMoO_6. The division of bulk modulus by shear modulus is referred to as Pugh's ratio [63], and this ratio provides insights into material behavior: ductile if (B/G) is greater than 1.75, and brittle if the reverse is true. The calculated Pugh's ratio values as tabulated in table 3 for both Ba_2MgReO_6 and Ba_2YMoO_6 are 2.43621 and 2.5112, respectively, suggesting a ductile nature with high malleability.

As detailed in equation (7), Cauchy's pressure, derived from the difference between C_{12} and C_{44}, can offer insights into the dominant type of bonds in a compound. When C_{12} is smaller than C_{44} (resulting in a negative C''), covalent bonds tend to dominate; otherwise, ionic bonds are more prominent [61]. Accordingly, the calculated Cauchy's pressure for both compounds is positive, signifying the prevalence of ionic bonds in their structures.

Additionally, the nature of the bonds can be further assessed through Poisson's ratio. This parameter characterizes a compound's behavior when compressed in one direction and expanding in two perpendicular directions. The value of Poisson's ratio is indicative of the type of bonding; typical covalent bonds exhibit values

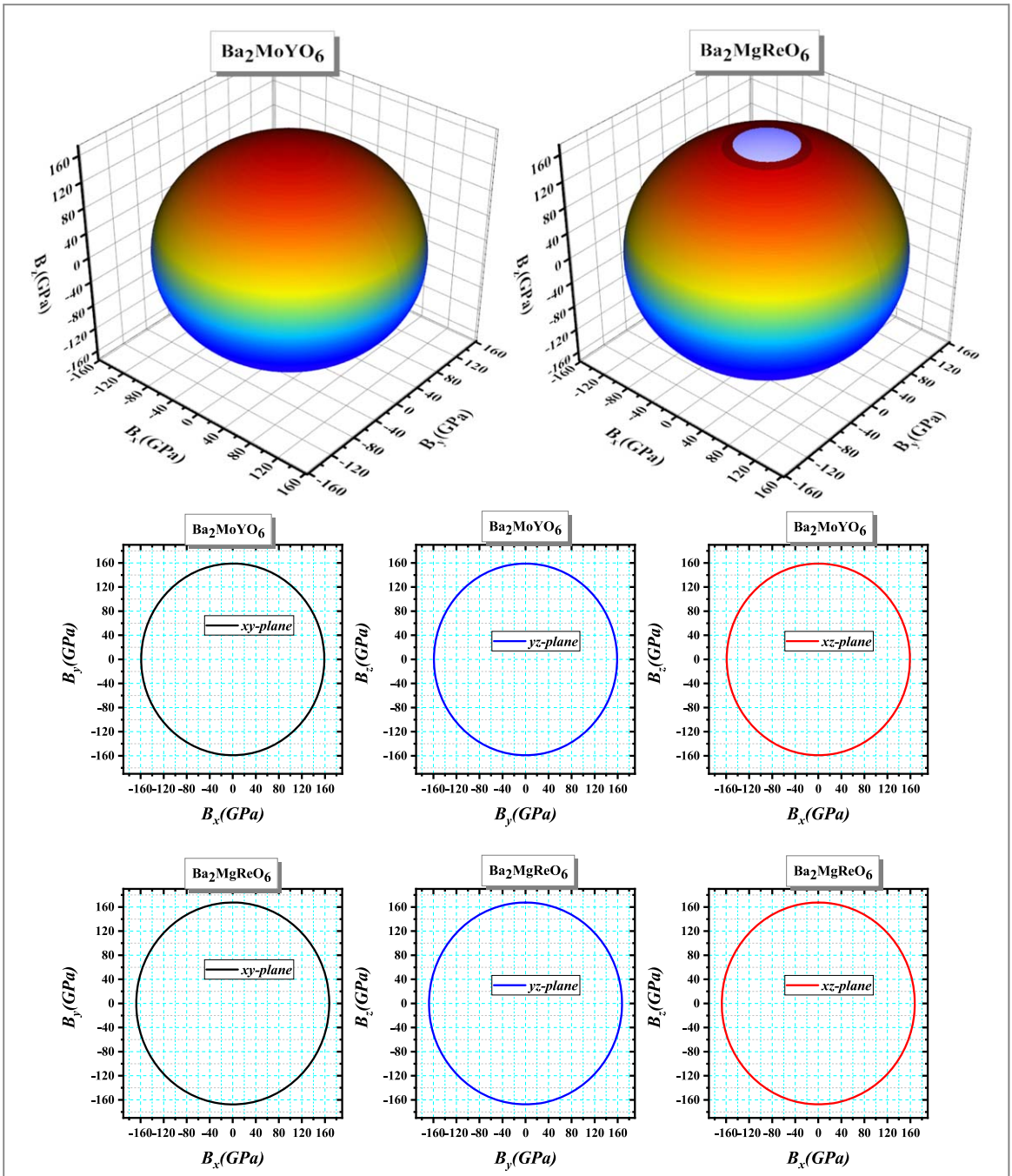

Figure 4. 3D visualizations of Bulk modulus of Ba_2MgReO_6 and Ba_2YMoO_6.

around 0.1, while for typical ionic crystals, the value can reach up to 0.25. In figure 6 our results reveal Poisson's coefficients exceeding 0.25, confirming that both compounds are primarily held together by ionic bonds.

One of the attributes derived from a material's elastic properties is its capacity to withstand alterations in length during longitudinal stretching or compression in a singular direction. This attribute is quantified by mathematical equation (4) and is referred to as Young's modulus. The comprehensive findings in table 3 and illustrate in figure 7 indicate that the Ba_2MgReO_6 compound possesses a greater propensity for longitudinal expansion than the Ba_2YMoO_6 compound.

Anisotropy constitutes another significant parameter that establishes whether the properties of alloys remain consistent across all directions during uniform stress-induced alterations in a material. When anisotropy equals unity, the crystal considered isotropic, whereas values differing from unity indicate variations in properties across different directions.

Our findings suggest the presence of anisotropy in both compounds. The Lame's parameters, λ and μ, were both computed using equations (9) and (10) respectively. Λ determines the material's compressibility, while μ

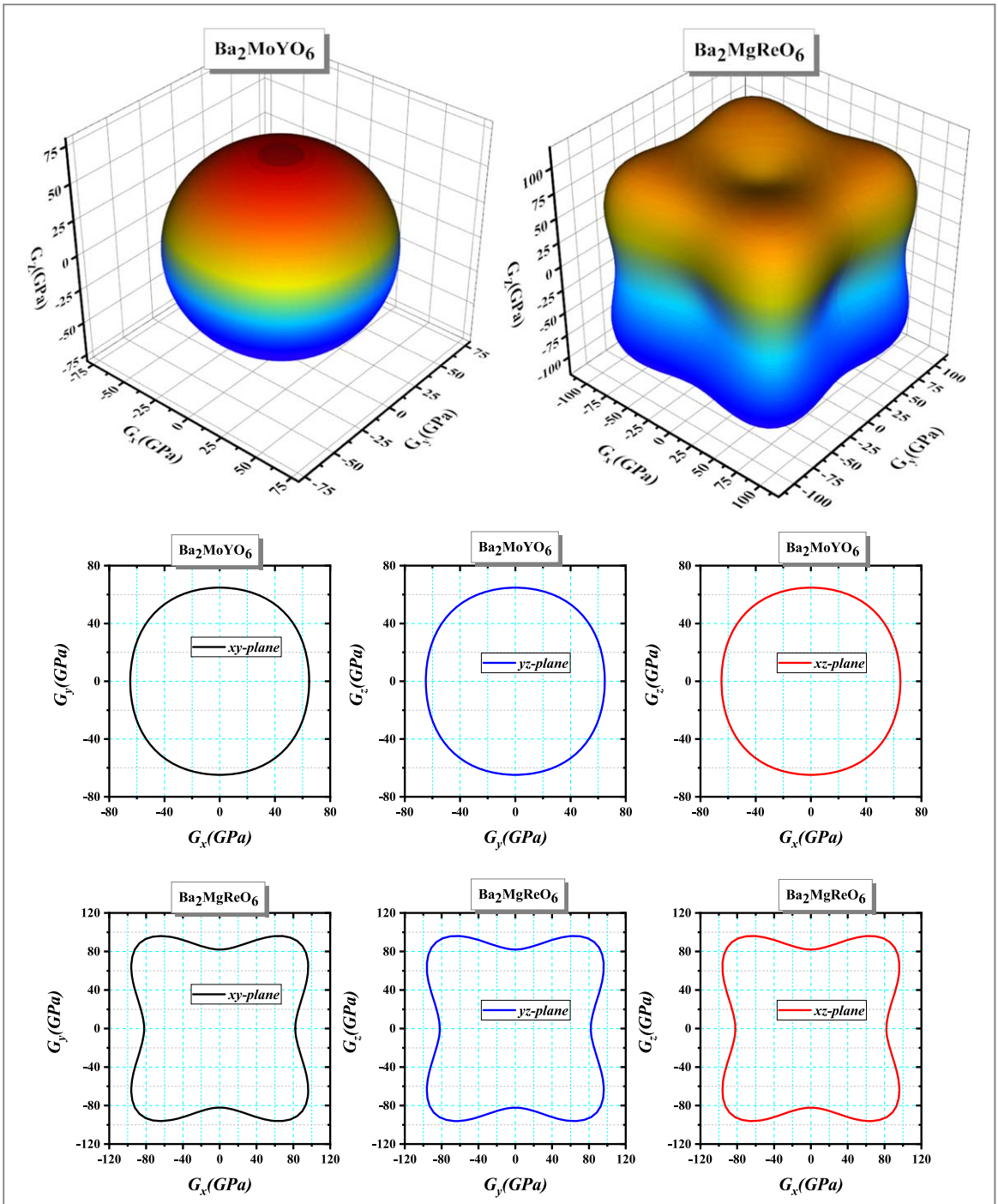

Figure 5. 3D visualizations of Shear modulus of Ba_2MgReO_6 and Ba_2YMoO_6.

represents its shear stiffness. In comparison, the Ba_2MgReO_6 double perovskite exhibits a higher shear coefficient and compressibility factor than Ba_2YMoO_6.

The Kleinman parameter (ξ) [64], calculated through equation (8), quantifies internal strain. Its value aids in determining the dominant type of bond, whether stretching or bending, within the compound's structure. Consequently, this parameter assists in ascertaining the overall nature of internal bonds, whether they predominantly involve stretching or bending. The compound's behavior is consequently influenced, resulting in either elongation or distortion. By analyzing the obtained Kleinman parameter values, it becomes evident that both Ba_2MgReO_6 and Ba_2YMoO_6 double perovskites are predominantly characterized by bond stretching.

Figures 4–7 express the 3D anisotropy of the bulk, shear, Young, and Poisson's modulus in various directions as well as their projections in xy, xz and yz planes. Through figure 4, it becomes evident that both Ba_2MgReO_6 and Ba_2YMoO_6 exhibit isotropic compressibility coefficients on all sides, as their three-dimensional closed surfaces take on a spherical shape. The compressibility coefficients for Ba_2MgReO_6 and

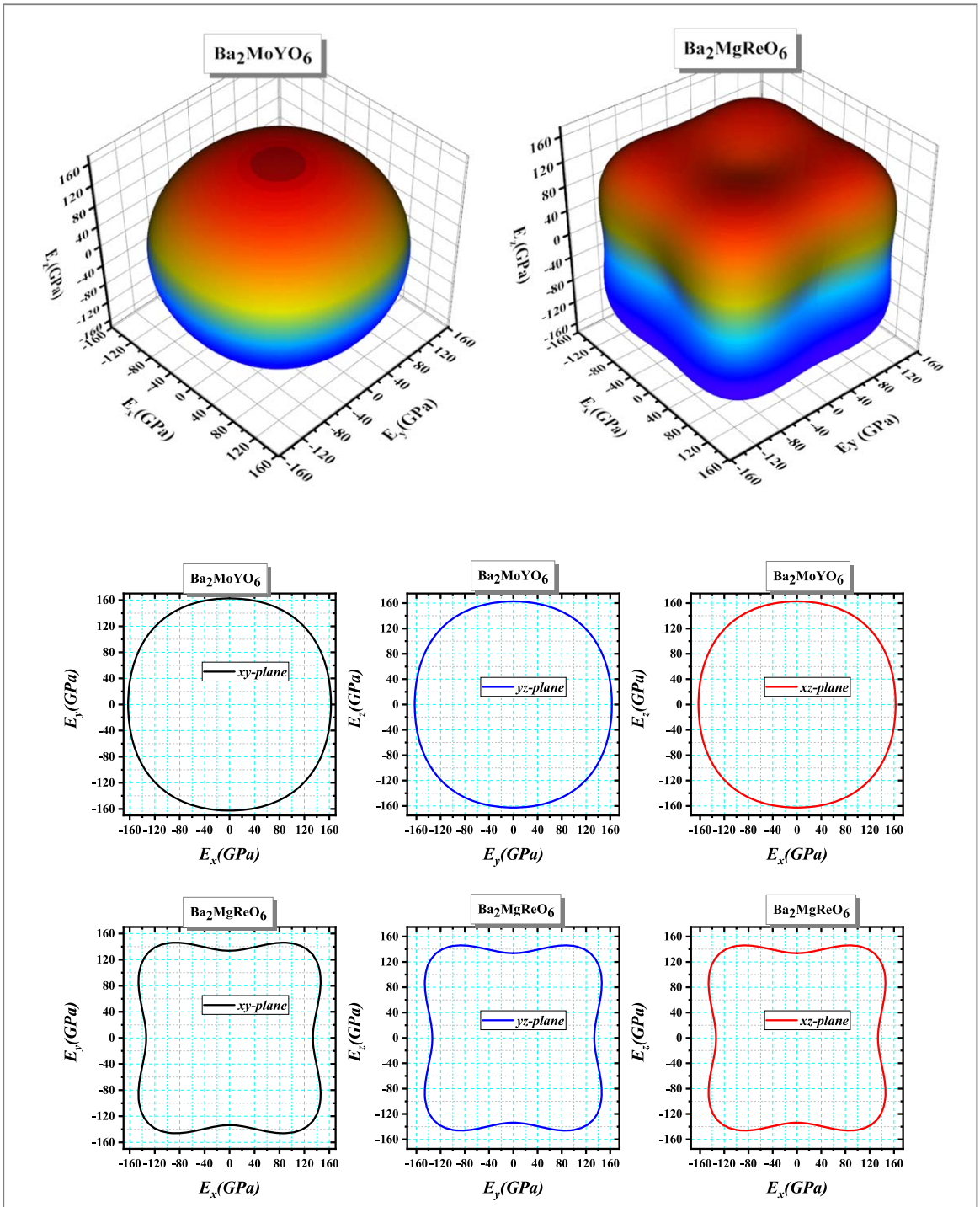

Figure 6. 3D visualizations of Young's modulus of Ba_2MgReO_6 and Ba_2YMoO_6.

Ba_2YMoO_6 are 160 and 165 GPa, respectively. Regarding the closed surfaces of the shear modulus in figure 5, it appears that the two compounds have different behavior, as the shear modulus of the compound Ba_2YMoO_6 is similar in all directions, unlike the compound Ba_2MgReO_6, where the cross-sections of the closed surfaces of the shear modulus show the presence of a concave convexity in the xy, xz, and yz planes, where the shear modulus decreases by 40 GPa in [100], [010] and [001] directions of the principal axes of the crystal lattice. The anisotropy in the elastic properties in the Ba_2MgReO_6 was also observed when drawing the closed surfaces of the Young modulus, as it was shown from figure 6 of Young's modulus in the three levels that there is a concave curvature of an amount not exceeding 15 GPa. This is the same observation that was recorded with regard to the Poisson coefficient, as the closed surfaces of the Poisson coefficient show convex curvatures in [100], [010] and [001] axes is 0.3 greater than the other directions.

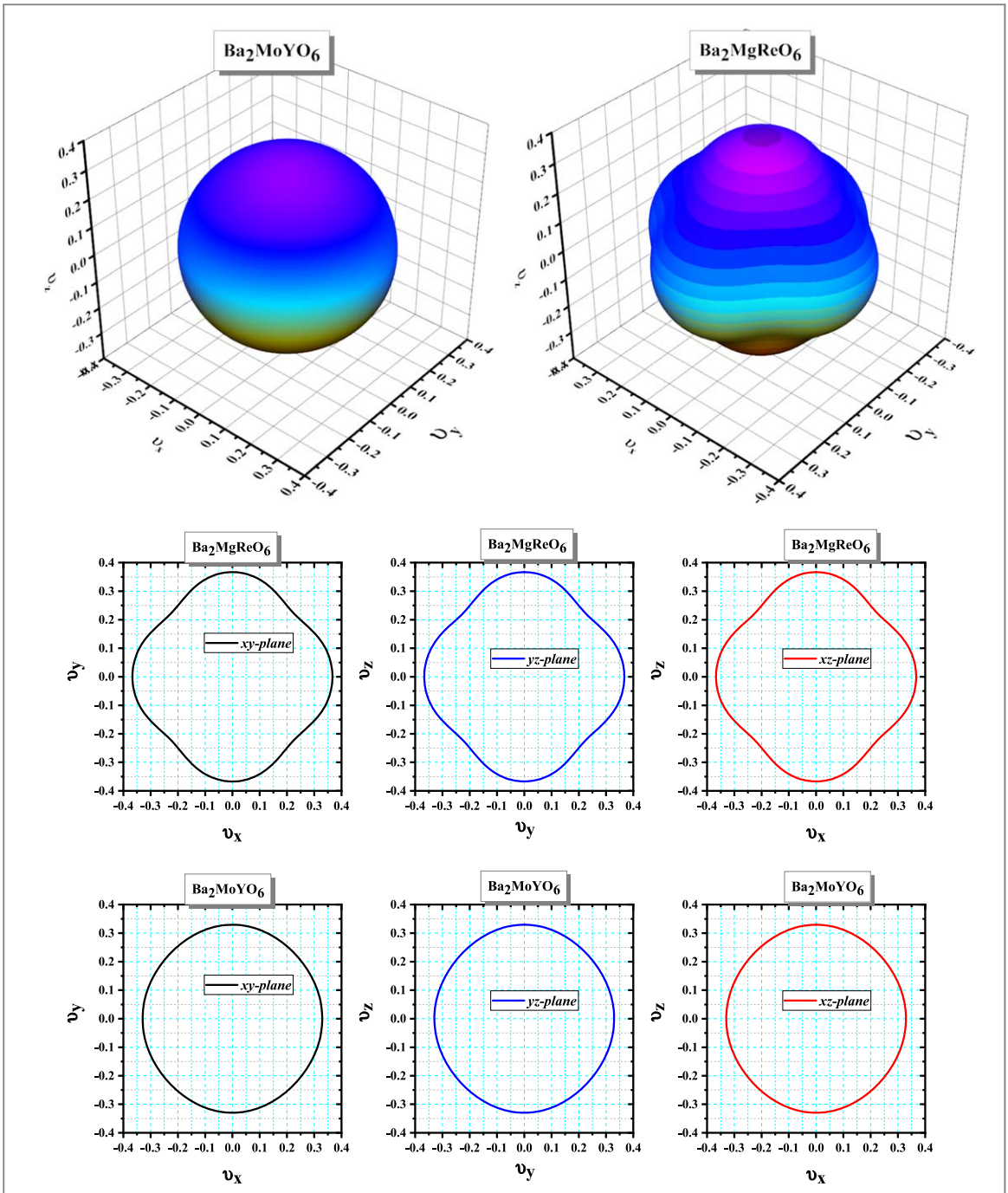

Figure 7. 3D visualizations of Young modulus of Ba_2MgReO_6 and Ba_2YMoO_6.

3.2. Electronic properties

Double perovskite compounds hold promise for diverse applications spanning energy conversion, catalysis, and electronic devices. Investigating their electronic properties is of paramount importance, as it provides insights into enhancing their characteristics and functionality, ultimately driving the advancement of double perovskite materials and facilitating the creation of novel applications.

The energy band arrangement of the two materials under examination was calculated at the high-symmetry locations within the initial Brillouin zone. As depicted in figure 8, the two compounds display contrasting behaviors. Remarkably, Ba_2MgReO_6 and Ba_2YMoO_6 both exhibit semiconductor properties in the spin-down state, revealing indirect energy gaps of 3.29 eV (L-δ) and 3.42 eV (λ-δ), respectively. In contrast, they display metallic characteristics in the spin-up state.

Utilizing the TB-mBJ approach, we calculated the densities of states, subsequently visualized in figure 9. The compounds under scrutiny exhibit two distinct bands conduction levels situated above the Fermi level and valence levels below separated by an indirect gap. The computed band gaps using the TB-mBJ approximation are

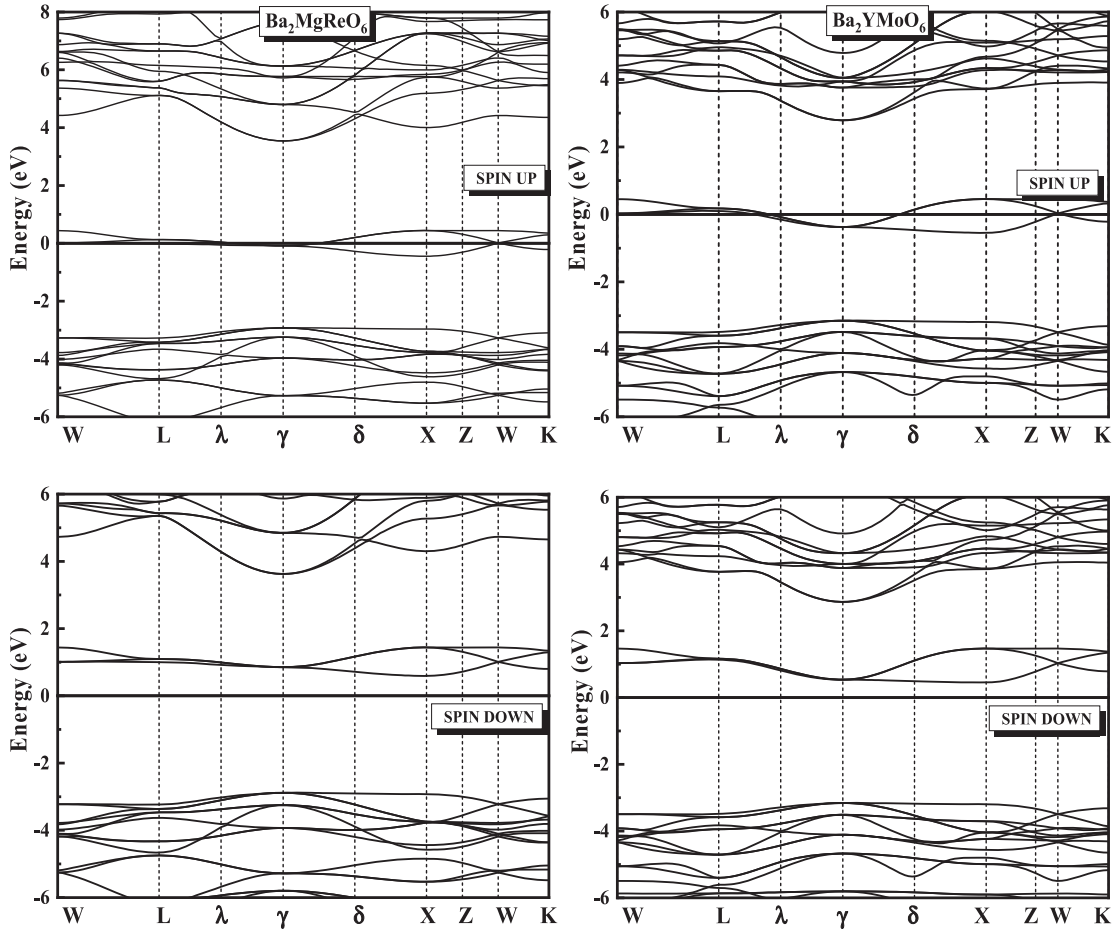

Figure 8. Band structure curves for Ba_2MgReO_6 and Ba_2YMoO_6 within the TB-mBJ approximation.

3.29 eV and 3.42 eV for Ba_2MgReO_6 and Ba_2YMoO_6, respectively. The investigated compounds in our study demonstrated band gaps in one spin orientation, affirming the presence of these dual bands. Specifically, in the spin-up direction, both Ba_2MgReO_6 and Ba_2YMoO_6 compounds manifest an overlap between conduction and valence bands, indicative of metallic characteristics. In contrast, in the spin-down direction, both compounds display an indirect band gap.

In dissecting the composition of each band within a band structure spectrum, we refer to the complete and partial density of states for the atomic orbitals in figure 9. These compounds exhibit semiconductor tendencies due to the absence of state density near the Fermi level. Specifically, in the cubic phase structure of Ba_2MgReO_6 and Ba_2YMoO_6, the conduction band primarily originates from the predominant contribution of the 'p' orbitals of the Barium atom, supplemented by a minor involvement from the 's' and 'd' orbitals of Ba. In contrast, the 'd' orbitals of Re and Y atoms and the 'p' orbitals of O exhibit a pronounced hybridization within the energy range of 2 eV to 8 eV.

3.3. Thermoelectric properties

Thermal energy can be directly transformed into electricity using thermoelectric materials. Double perovskite materials, which efficiently convert heat to electricity and have strong heat absorption, are promising for this purpose. Utilizing Boltzmann transport theory through the BoltzTraP program [55], the thermoelectric traits of these compounds are computed, yielding the final values. The conversion efficiency of thermoelectric devices, quantified by the ZT figure of merit, is currently low. ZT is defined as:

$$ZT = S^2\frac{\sigma T}{k}$$

The inherent Seebeck coefficient of a material indicates how the voltage across the material's terminals is linked to the applied temperature gradient. This temperature difference causes the movement of charge carriers within the material, like electrons or holes [65, 66], leading to the creation of an electric current. Most of the

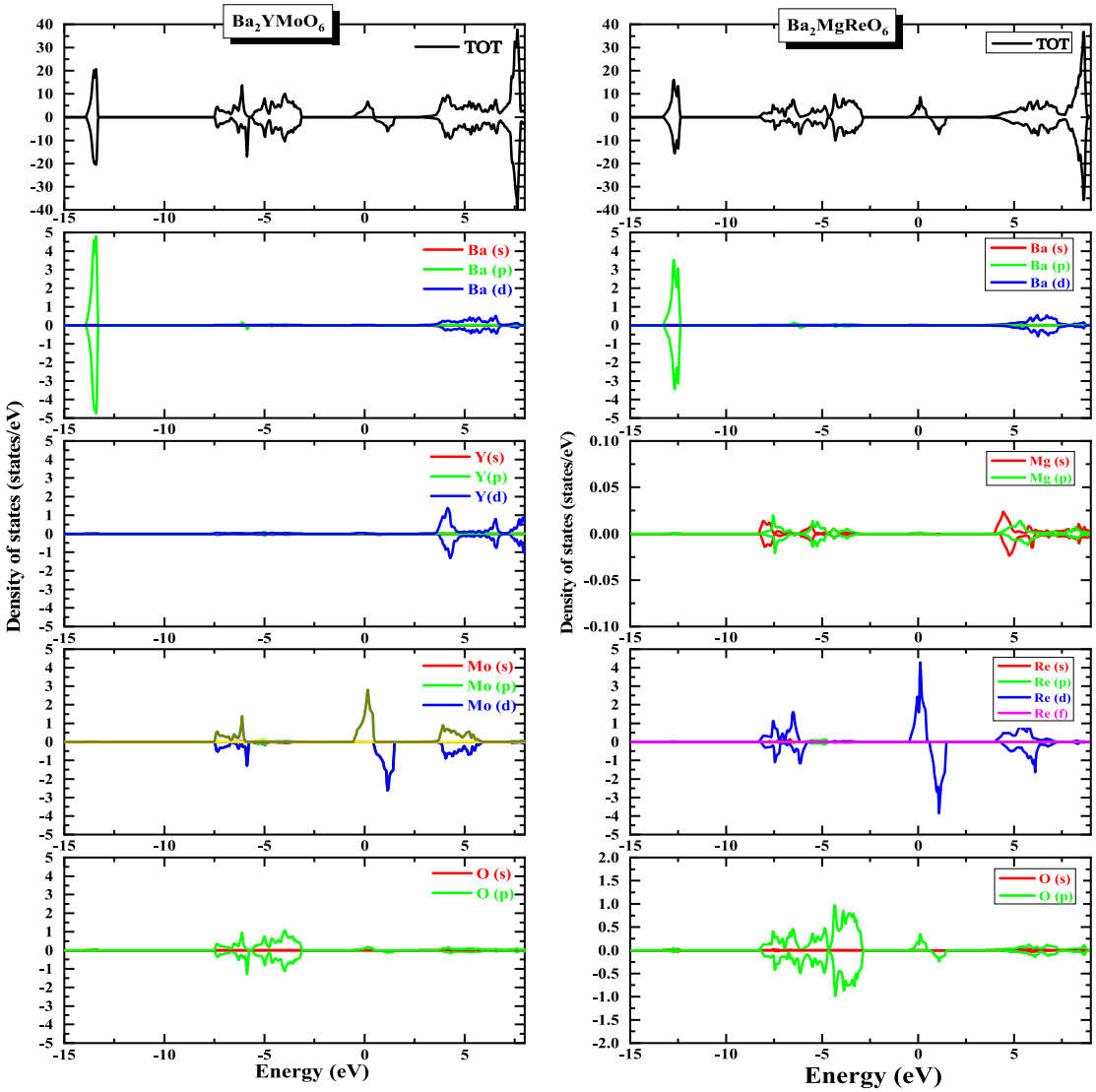

Figure 9. The calculated total and partial density of states for both Ba_2MgReO_6 and Ba_2YMoO_6 within the TB-mBJ approximation.

thermoelectric parameters were studied in this section, their changes as a function of the concentration of each of the charge carriers (holes and electrons) in a temperature range of up to 1000 K. Regarding the Seebeck coefficient for both compounds, the obtained results in figure 10 showed that an increase in temperature above 600 K would raise the Seebeck coefficient for holes and electrons to a value greater than 0.5 mV K^{-1}, while increasing the concentration of charge carriers raises the Seebeck coefficient for holes and lowers it for electrons. Regarding the contribution of charge carriers to thermal and electrical conductivity, it was studied by addressing the electrical and thermal conductivity of holes and electrons. The electrical conductivity of electrons is greater than that of holes, as its value can exceed $1.1\times10^{6}\,\Omega^{-1}cm^{-1}$ and $1.3\times10^{6}\,\Omega^{-1}cm^{-1}$ for Ba_2YMoO_6 and Ba_2MgReO_6 compounds, respectively, when they are doped with a concentration of electrons of 10^{21} cm^{-3} at room temperature. As for thermal conductivity, its value increases with increasing temperature for both electrons and holes.

The figure of merit and the power factor are two important properties to detect the ability and efficiency of materials in thermoelectric conversion, in addition to the possibility of determining through them the type of charge carriers and the optimal doping concentration of the materials, as well as the optimal thermal field to obtain high efficiency. The curves of changes in the figure of merit and the power factor estimate that holes have a better thermoelectric capacity than electrons, as doping both Ba_2MgReO_6 and Ba_2YMoO_6 at a concentration of 10^{21} cm^{-3} of the holes at temperatures ranging from 300 to 500 K would lead to a figure of merit of up to 0.4. With a power factor exceeding 5.2×10^{6} $W.cm^{-1}.s^{-1}.K^{-2}$. From the results obtained, we can conclude that both compounds prefer holes doping (p-type), as they have weak thermoelectric properties.

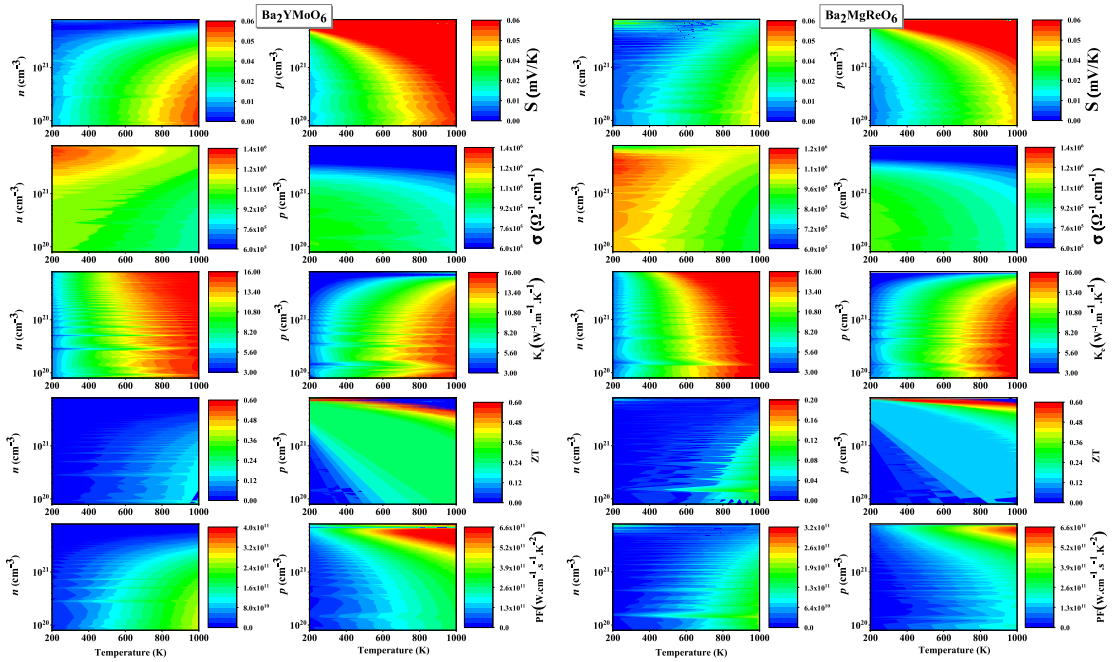

Figure 10. Changes in the Seebeck coefficient (S), electrical conductivity (σ/τ), thermal conductivity (κ/τ), electronic specific heat capacity (c), figure of merit (ZT), and power factor (PF) for Ba_2MgReO_6 and Ba_2YMoO_6 compounds as a function of holes and electrons concentrations and temperature.

4. Conclusion

The current investigation encompasses the determination of the structural robustness, electronic properties, elastic behavior, and thermoelectric traits of double perovskite compounds. These materials exhibit stability within the cubic structure, adhering to the spatial symmetry dictated by the Fm-3m space group. This stability within the Fm-3m space group is ascertained through energy optimization and the tolerance factor. Additionally, the positive values of elastic constants serve as confirmation of the mechanical endurance of the materials. These elastic constants further affirm the materials' ductile and anisotropic characteristics. The examination of the band structure and density of states underscores their semiconducting nature characterized by a slight indirect band gap. The notable combination of high Seebeck coefficient and low thermal conductivity contributes to an elevated figure of merit, nearing unity. Our discoveries also propose the potential suitability of Ba_2MgReO_6 and Ba_2YMoO_6 as candidates for thermoelectric applications, considering their distinctive attributes, which were supported by evaluating their thermoelectric properties via the semi-classical Boltzmann theory. Nevertheless, in a broader sense, our outcomes align with other theoretical investigations, thus reinforcing the feasibility of employing these compounds across diverse applications.

Data availability statement

No new data were created or analysed in this study.

ORCID iDs

Mohammed Elamin Ketfi https://orcid.org/0000-0002-6725-7703
Saber Saad Essaoud https://orcid.org/0000-0002-6337-3184
Anas Y Al-Reyahi https://orcid.org/0000-0001-8662-5543
Ahmad A Mousa https://orcid.org/0000-0003-4256-2055
Nabil Al-Aqtash https://orcid.org/0000-0003-0850-4580

References

[1] Ravi S 2020 High Curie temperature and room temperature magnetoresistance in Pr2FeCrO6 material for spintronics applications *Mater. Lett.* **278** 128448
[2] Xu X, Zhong Y and Shao Z 2019 Double perovskites in catalysis, electrocatalysis, and Photo(electro)catalysis *Trends Chem.* **1** 410–24

[3] Klyndyuk A I, Chizhova E A, Kharytonau D S and Medvedev D A 2021 Layered oxygen-deficient Double Perovskites as promising cathode materials for solid oxide fuel cells *Materials* **15** 141
[4] Mahmood Q, Hassan M, Yousaf N, AlObaid A A, Al-Muhimeed T I, Morsi M, Albalawi H and Alamri O A 2022 Study of lead-free double perovskites halides Cs2TiCl6, and Cs2TiBr6 for optoelectronics, and thermoelectric applications *Mater. Sci. Semicond. Process.* **137** 106180
[5] Mohanty D and Hung I-M 2023 *Perovskites for Fuel Cell Applications Perovskite Metal Oxides* (Amsterdam: Elsevier) 395–418
[6] Karwasara H, Bhamu K C, Kang S G, Kushwaha A K, Rai D P, Sappati S, Sahariya J and Soni A 2022 Ab-initio investigations for structural, mechanical, optoelectronic, and thermoelectric properties of Ba2SbXO6 (X Nb, Ta) compounds *J. Alloys Compd.* **893** 162332
[7] Vasala S and Karppinen M 2015 A2B′B″O6 perovskites: a review *Prog. Solid State Chem.* **43** 1–36
[8] Grätzel M 2014 The light and shade of perovskite solar cells *Nat. Mater.* **13** 838–42
[9] Stoumpos cc, Malliakas C D and Kanatzidis M G 2013 Semiconducting Tin and Lead Iodide Perovskites with Organic Cations: Phase Transitions, High Mobilities, and Near-Infrared Photoluminescent Properties *Inorg. Chem.* **52** 9019–38
[10] Baikie T, Fang Y, Kadro J M, Schreyer M, Wei F, Mhaisalkar S G, Graetzel M and White T J 2013 Synthesis and crystal chemistry of the hybrid perovskite (CH3NH3)PbI3 for solid-state sensitised solar cell applications *J. Mater. Chem. A* **1** 5628
[11] Hao F, Stoumpos cc, Cao D H, Chang R P H and Kanatzidis M G 2014 Lead-free solid-state organic–inorganic halide perovskite solar cells *Nat. Photonics* **8** 489–94
[12] Benamer A, Medkour Y, Essaoud S S, Chaddadi S and Roumili A 2021 Ab-initio study of the structural, electronic, elastic and thermodynamic properties of Sc3XB (X= Sn, Al, Hf) *Solid State Commun.* **331** 114305
[13] Mouna S C, Radjai M, Bouhemadou A, Houatis D, Allali D, Essaoud S S and Bin-Omran S 2023 Structural, elastic, and thermodynamic properties of BaXCl3 (X= Li, Na) perovskites under pressure effect: *ab initio* exploration *Phys. Scr.* **98** 065949
[14] Sâad Essaoud S, Bouhemadou A, Maabed S, Bin-Omran S and Khenata R 2022 Pressure dependence of the electronic, optical, thermoelectric, thermodynamic properties of CsVO3: first-principles study *Philos. Mag.* **102** 1–25
[15] Nadeem J, Kiran Z, Zeba I, Gulzar F, Awais M and Gillani S S A 2023 A detailed computational study to investigate the influence of metals (Bi, Sn, Tl) substitution on phase transition, electronic band structure and their implications on optical, elastic, anisotropic and mechanical properties of PbHfO3 *Opt. Quantum Electron.* **55** 45
[16] You J, Li G, Zhang S, Zhang X, Luo J, Rao M and Peng Z 2021 Synthesis, characterization and thermodynamic properties of KNbO3 *J. Alloys Compd.* **882** 160641
[17] Mahmood Q, Yaseen M, Hassan M, Rashid M S, Tlili I and Laref A 2019 The first-principle study of mechanical, optoelectronic and thermoelectric properties of CsGeBr3 and CsSnBr3 perovskites *Mater. Res. Express* **6** 045901
[18] Behera D, Dixit A, Kumari K, Srivastava A, Sharma R, Mukherjee S K, Khenata R, Boumaza A and Bin-Omran S 2022 Structural, elastic, mechanical, and thermodynamic characteristic of NaReO3 and KReO3 perovskite oxides from first principles study *Eur. Phys. J. Plus* **137** 1345
[19] Zheng W, Cheng H, Liu Y, Chen L, Guo Y, Yang Y, Yan X H and Wu D 2022 Machine learning for imbalanced datasets: application in prediction of 3d-5d double perovskite structures *Comput. Mater. Sci.* **209** 111394
[20] Bhalla A S, Guo R and Roy R 2000 The perovskite structure—a review of its role in ceramic science and technology *Mater. Res. Innov.* **4** 3–26
[21] Chanda S, Maity R, Saha S, Dutta A and Sinha T P 2021 Double perovskite nanostructured Dy2CoMnO6 an efficient visible-light photocatalysts: synthesis and characterization *J. Sol-Gel Sci. Technol.* **99** 600–13
[22] Sâad Essaoud S, Al Azar S M, Mousa A A and Al-Reyahi A Y 2023 DFT-Based investigation of electronic-structure, magnetic and thermoelectric properties of Dy2CoMnO6 double perovskite *Phys. Scr.* **98** 075930
[23] Bhatti I N, Bhatti I N, Mahato R N and Ahsan M A H 2020 Physical properties in nano-crystalline Ho2CoMnO6 *Ceram. Int.* **46** 46–55
[24] Younas M, Mahmood Q, Kattan N A, Alshahrani T, Mera A, Amin M A, Mersal G A and Somaily H H 2022 Study of new double perovskites Tl2PtX6 (X= Cl, Br, I) for solar cells and thermoelectric applications *Phys. Scr.* **97** 125803
[25] Ramawat S, Kukreti S, Kale A J, Dutt R, Chakrabarti A and Dixit A 2023 Cs2KMnCl6: a possible half-metallic double perovskite for spintronics *J. Appl. Phys.* **133**
[26] Aqtash N A, Al Azar S M, Al-Reyahi A Y, Mufleh A, Maghrabi M, Essaoud S S, Berarma K and Mousa A A 2023 First-principles calculations to investigate structural, mechanical, electronic, optical, and thermoelectric properties of novel cubic double Perovskites X2AgBiBr6 (X= Li, Na, K, Rb, Cs) for optoelectronic devices *Mol. Simul.* **49** 1–12
[27] Djefal A, Amari S, Obodo K O, Beldi L, Bendaoud H, Evans R F L and Bouhafs B 2017 Half-Metallic Ferromagnetism in Double Perovskite Ca_2CoMoO_6 Compound: DFT+U Calculations *SPIN* **07** 1750009
[28] Borges R P, Thomas R M, Cullinan C, Coey J M D, Suryanarayanan R, Ben-Dor L, Pinsard-Gaudart L and Revcolevschi A 1999 Magnetic properties of the double perovskites A_2FeMoO_6; A = Ca, Sr, Ba *J. Phys. Condens. Matter* **11** L445–50
[29] Mitchell R H 2002 By Roger H. Mitchell. Thunder Bay, Ontario: Almaz Press, 2002. Price USD 70.00. ISBN 0-9689411-0-9
[30] Anderson M, Greenwood K, Taylor G and Poeppelmeier K 1993 B-cation arrangements in double perovskites *Prog. Solid State Chem.* **22** 197–233
[31] King G and Woodward P M 2010 Cation ordering in perovskites *J. Mater. Chem.* **20** 5785
[32] Davies P K, Wu H, Borisevich A Y, Molodetsky I E and Farber L 2008 Crystal Chemistry of Complex Perovskites: New Cation-Ordered Dielectric Oxides *Annu. Rev. Mater. Res.* **38** 369–401
[33] Howard C J, Kennedy B J and Woodward P M 2003 Ordered double perovskites—a group-theoretical analysis *Acta Crystallogr. B* **59** 463–71
[34] Goodenough J B 2004 Electronic and ionic transport properties and other physical aspects of perovskites *Rep. Prog. Phys.* **67** 1915–93
[35] Serrate D, Teresa J M D and Ibarra M R 2007 Double perovskites with ferromagnetism above room temperature *J. Phys. Condens. Matter* **19** 023201
[36] Karppinen M and Yamauchi H 2005 Chemistry of halfmetallic and related cation-ordered double perovskites *Frontiers in Magnetic Materials* ed A V Narlikar (Berlin: Springer) 153–84
[37] Chen S H, Xiao Z R, Liu Y P and Wang Y K 2013 Investigation of Possible Half-Metallic antiferromagnets on double perovskites $A_2BB'O_6$ (A =Ca, Sr Ba; B,B'=transition metal elements) *Commun. Comput. Phys.* **13** 526–39
[38] Mir S A and Gupta D C 2021 Scrutinizing the stability and exploring the dependence of thermoelectric properties on band structure of 3d-3d metal-based double perovskites Ba2FeNiO6 and Ba2CoNiO6 *Sci. Rep.* **11** 10506
[39] Kubel F, Wandl N, Pantazi M, D'Anna V and Hagemann H 2013 The Periodate-based double Perovskites M_2NaIO_6 (M = Ca, Sr, and Ba) *Z Für Anorg. Allg. Chem.* **639** 892–8

[40] Wu H 2001 Electronic structure study of double perovskites A 2 FeReO 6 (A = B a , S r , C a) and Sr 2 M MoO 6 (M = C r , M n , F e , C o) by LSDA and LSDA + U *Phys. Rev. B* **64** 125126
[41] Jeon B C *et al* 2010 Electronic structure of double perovskite A_2FeReO_6 (A = Ba and Ca): interplay between spin–orbit interaction, electron correlation, and lattice distortion *J. Phys. Condens. Matter* **22** 345602
[42] Chen Q, De Marco N, Yang Y (M), Song T-B, Chen C-C, Zhao H, Hong Z, Zhou H and Yang Y 2015 Under the spotlight: The organic–inorganic hybrid halide perovskite for optoelectronic applications *Nano Today* **10** 355–96
[43] Aharen T *et al* 2010 Magnetic properties of the geometrically frustrated S = 1 2 antiferromagnets, La 2 LiMoO 6 and Ba 2 YMoO 6 , with the B-site ordered double perovskite structure: Evidence for a collective spin-singlet ground state *Phys. Rev. B* **81** 224409
[44] Aharen T *et al* 2010 Structure and magnetic properties of the S = 1 geometrically frustrated double perovskites La 2 LiReO 6 and Ba 2 YReO 6 *Phys. Rev. B* **81** 064436
[45] De Vries M A, Mclaughlin A C and Bos J-W G 2010 Valence bond glass on an fcc lattice in the Double perovskite Ba 2 YMoO 6 *Phys. Rev. Lett.* **104** 177202
[46] Carlo J P *et al* 2011 Triplet and in-gap magnetic states in the ground state of the quantum frustrated fcc antiferromagnet Ba2YMoO6 *Phys. Rev. B - Condens. Matter Mater. Phys.* **84** 29–32
[47] Bramnik K G, Ehrenberg H, Dehn J K and Fuess H 2003 Preparation, crystal structure, and magnetic properties of double perovskites M2MgReO6 (M = Ca, Sr, Ba) *Solid State Sci.* **5** 235–41
[48] Dar S A, Srivastava V, Sakalle U K and Pagare G 2018 Insight into electronic structure, magnetic, mechanical and thermodynamic properties of double perovskite Ba2MgReO6: A first-principles investigation *Comput. Condens. Matter* **14** 137–43
[49] Hirai D and Hiroi Z 2019 Successive symmetry breaking in a Jeff = 3/2 quartet in the spin–orbit coupled insulator Ba2MgReO6 *J. Phys. Soc. Jpn.* **88** 1–8
[50] Marjerrison C A *et al* 2016 Cubic Re6+ (5d1) Double Perovskites, Ba2MgReO6, Ba2ZnReO6, and Ba2Y2/3ReO6: Magnetism, Heat Capacity, μsR, and neutron scattering studies and comparison with theory *Inorg. Chem.* **55** 10701–13
[51] Chen G, Pereira R and Balents L 2010 Exotic phases induced by strong spin–orbit coupling in ordered double perovskites *Phys. Rev. B - Condens. Matter Mater. Phys.* **82** 1–25
[52] Blaha P, Schwarz K, Tran F, Laskowski R, Madsen G K H and Marks L D 2020 WIEN2k: An APW+lo program for calculating the properties of solids *J. Chem. Phys.* **152** 074101
[53] Perdew J P, Burke K and Ernzerhof M 1996 Generalized Gradient approximation Made Simple *Phys. Rev. Lett.* **77** 3865–8
[54] Becke A D and Johnson E R 2006 A simple effective potential for exchange *J. Chem. Phys.* **124** 221101
[55] Madsen G K H and Singh D J 2006 BoltzTraP. A code for calculating band-structure dependent quantities *Comput. Phys. Commun.* **175** 67–71
[56] Martínez-Lope M J, Alonso J A and Casais M T 2003 Synthesis, crystal and magnetic structure of the double perovskites A_2NiMoO_6 (A = Sr, Ba): a neutron diffraction study *Eur. J. Inorg. Chem.* **2003** 2839–44
[57] Marjerrison C A, Thompson C M, Sala G, Maharaj D D, Kermarrec E, Cai Y, Hallas A M, Wilson M N, Munsie T J and Granroth G E 2016 Cubic Re6+ (5d1) double perovskites, Ba2MgReO6, Ba2ZnReO6, and Ba2Y2/3ReO6: magnetism, heat capacity, μSR, and neutron scattering studies and comparison with theory *Inorg. Chem.* **55** 10701–13
[58] Yu C-J, Ri I-C, Ri H-M, Jang J-H, Kim Y-S and Jong U-G 2023 First-principles study on structural, electronic and optical properties of halide double perovskite Cs_2AgBX_6 (B = In, Sb; X = F, Cl, Br, I) *RSC Adv.* **13** 16012–22
[59] Essaoud S S, Al Azar S M, Mousa A A and Masharfe R S 2023 Characterization of structural, dynamic, optoelectronic, thermodynamic, mechanical and thermoelectric properties of AMgF3 (A= K or Ag) fluoro-perovskites compounds *Phys. Scr.* **98** 035820
[60] Mouhat F and Coudert F-X 2014 Necessary and sufficient elastic stability conditions in various crystal systems *Phys. Rev. B* **90** 224104
[61] Mousa A A, Al Azar S M, Essaoud S S, Berarma K, Awad A, Mahmoud N T, Jaradat E K and Abu-Jafar M S 2022 Structural, elastic, electronic, magnetic, and thermoelectric characteristics of MgEu2X4 (X= S, Se) spinel compounds: ab-initio calculations *Phys. Status Solidi b* **259** 2200191
[62] Sâad Essaoud S and Jbara A S 2021 First-principles calculation of magnetic, structural, dynamic, electronic, elastic, thermodynamic and thermoelectric properties of Co2ZrZ (Z = Al, Si) Heusler alloys *J. Magn. Magn. Mater.* **531** 167984
[63] Pugh S F 1954 XCII. Relations between the elastic moduli and the plastic properties of polycrystalline pure metals *Lond. Edinb. Dublin Philos. Mag. J. Sci.* **45** 823–43
[64] Kleinman L 1962 Deformation Potentials in Silicon. I. Uniaxial Strain *Phys. Rev.* **128** 2614–21
[65] Sâad Essaoud S, Bouhemadou A, Ketfi M E, Allali D and Bin-Omran S 2023 Structural parameters, electronic structure and linear optical functions of LuXCo2Sb2 (X = V, Nb and Ta) double half Heusler alloys *Phys. B Condens. Matter* **657** 414809
[66] Ketfi M E, Essaoud S S, Al Azar S, Al-Reyahi A Y, Mousa A A and Mufleh A 2023 Insight into the spin-polarized structural, optoelectronic, magnetic, thermodynamic, and thermoelectric properties of PdBO2 (B = Al, Cr, and Rh) Delafossite semiconductor *Opt. Quantum Electron.* **55** 1013